Helimagnetic structures in epitaxial Nd/Y superlattices and alloys

B. A. Everitt* and M. B. Salamon
Department of Physics, University of Illinois at Urbana-Champaign, 1110 West Green Street, Urbana, Illinois 61801

J. A. Borchers and R. W. Erwin
Reactor Division, National Institute of Standards and Technology, Gaithersburg, Maryland 20899

J. J. Rhyne
Missouri University Research Reactor, Columbia, Missouri 65211

B. J. Park and K. V. O'Donovan
Department of Physics, University of Illinois at Urbana-Champaign, 1110 West Green Street, Urbana, Illinois 61801

D. F. McMorrow
Risø National Labratory, DK-4000 Roskilde, Denmark

C. P. Flynn
Department of Physics, University of Illinois at Urbana-Champaign, 1110 West Green Street, Urbana, Illinois 61801
(Received 6 February 1997)

The complex magnetic structure of Nd exhibits a new magnetic phase when grown epitaxially, either as a stabilized double hexagonal close-packed alloy, or as part of a Nd/Y superlattice. In the alloy and in those superlattices with small Nd/Y ratios, the incommensurate *b* axis modulated structure exhibited by elemental Nd at $T_N = 19.9$ K is absent. In its place, incommensurate helimagnetic order, similar to that in dilute yttrium alloys of the heavy lanthanides, appears below approximately 30 K. Evidence for coherent propagation of the magnetic spiral through the Y spacers is observed in some Y-rich superlattices. As the Nd:Y ratio in the superlattices is increased, the *b* axis modulated phases reappear and coexist with the helical phase. Thick epitaxial Nd films, nevertheless, exhibit only bulklike magnetic structure. We discuss these observations in terms of band structure modifications. [S0163-1829(97)01133-8]

I. INTRODUCTION

The element neodymium orders magnetically below $\simeq 19.9$ K and exhibits one of the most complex magnetic structures known, involving multiple, incommensurate magnetization waves.[1] Unlike the heavier rare earths, the periodicities **q** of these waves are not obviously related to features in the electronic band structure, nor is the confinement of the magnetic moments in the basal planes the obvious consequence of crystal field effects. Rather, the magnetic structure is the result of a delicate balance among indirect exchange, anisotropic two-ion coupling, and crystal field effects.[2] Under such circumstances, it is likely that the coherency strains that accompany epitaxial growth will significantly alter the magnetic transition temperatures and phases. Indeed, we have shown[3] that coherency strain and clamping to a substrate, through their effect on magnetostriction, profoundly affect the magnetic properties of heavy rare-earth superlattices and thin films.

Unlike the heavy lanthanides, Nd orders in a double hexagonal close-packed (dhcp) structure. The Fermi-surface nesting features that lead to helimagnetism in, e.g., Dy or Ho, are absent in the dhcp structure, suggesting that this feature drives dhcp crystallization in the light rare earths.[4] Nd-Y alloys exhibit dhcp structure to approximately 30% Y and are hcp beyond 40% Y. The samarium (nine-layer repeat) structure appears in the intermediate concentration range. Sharif and Coles[5] found alloys in that intermediate concentration to contain a significant fraction of a metastable magnetic phase with a transition near 32 K. At the Nd-rich end, Zochowski *et al.*[6] found that 6 at. % of Y suppresses the ''archipelago'' of magnetic satellites present in bulk Nd. In this study, we report magnetization and neutron scattering measurements of *c*-axis Nd/Y superlattices,[7] a $Nd_{0.62}Y_{0.38}$ alloy, and a thick Nd film, all grown by molecular beam epitaxy. Nd and Y are exceptionally well lattice matched in the basal plane, with a 0.24% mismatch at room temperature providing compressive strain on the Nd layers. The thick Nd film exhibits a multiple-**q** behavior similar to that of bulk Nd, but a different magnetic structure appears in superlattices and coexists with the bulklike structure. Only this different magnetic structure is observed in the epitaxial alloy and, in both superlattices and the alloy, this phase persists to temperatures above 30 K. We suggest that this phase is the source of the susceptibility peak found at 32 K by Sharif and Coles in their quenched $Nd_{0.63}Y_{0.37}$ alloy, and will argue that this phase arises from a modification of the band structure relative to pure Nd rather than as a consequence of epitaxial strain.

The magnetic structure of Nd has been studied extensively; a comprehensive review of the current state of understanding has been published recently by Lebech *et al.*[8] The *ABAC* stacking sequence of the dhcp structure provides two

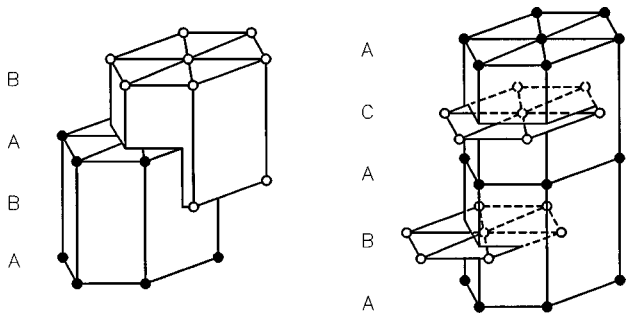

FIG. 1. The hcp (left) and dhcp (right) crystal structures. In the latter, for an ideal close-packed c/a ratio, the B- and C-plane sites have hexagonal symmetry; the A-plane sites have local cubic symmetry. (From Ref. 2.)

distinct crystallographic environments: hexagonal local arrangements in the B and C layers and a nearly cubic environment in the A layer, as shown in Fig. 1. The hexagonal sites order magnetically at $T_N = 19.9$ K into a longitudinal, single-**q** structure, with both the propagation wave vector **q** and the modulated magnetic moments parallel to one of the hexagonal **b**$(10\cdot 0)$ axes. Three possible domains coexist, giving rise to six magnetic reflections in neutron scattering, as shown in Fig. 2(a). Below 19.1 K the moments turn away from the **b** axis and a perpendicular component of **q** develops parallel to **a**$(11\cdot 0)$. This leads to a transverse splitting of the magnetic satellites and a ''double-**q**'' structure, as shown in Fig. 2(b). Below 8.2 K order begins to develop on the cubic sites, with a different wave vector $\mathbf{q}_3$, as shown in Fig. 2(c). The lowest temperature phase arises below 6.2 K, in which $\mathbf{q}_1$ and $\mathbf{q}_2$ are split longitudinally along **b** while the cubic-site modulation exhibits a fourfold splitting, as sketched in Fig. 2(d). The moment on the hexagonal sites is $2.67 \pm 0.02 \mu_B$/atom at the temperature at which the cubic sites order. When the cubic sites order, the total moment in both modulated structures remains at $2.67 \mu_B$/atom.[9] Some, but not all, aspects of this complex behavior are retained in epitaxial samples, and new features appear.

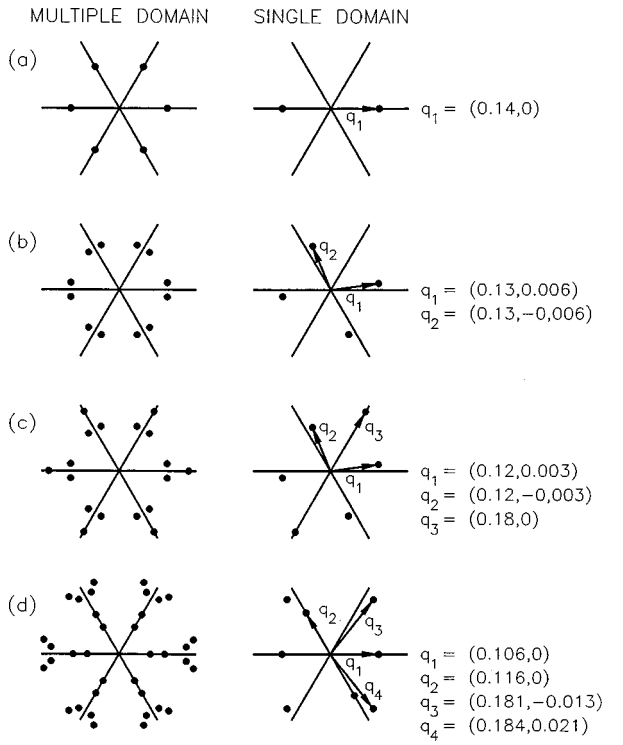

FIG. 2. Magnetic satellites observed in a $(00\cdot l)$ plane, for l odd, in Nd. The **q** vectors at different temperatures are specified as components parallel and perpendicular to one of the **a*** axes. [Adapted from R. M. Moon and R. M. Nicklow, J. Magn. Magn. Mater. **100**, 139 (1991).]

In Sec. II we describe the preparation and initial characterization of the epitaxial samples. We present the neutron scattering data in Sec. III, comparing and contrasting it with the results summarized above for elemental Nd. Finally, we discuss the results and suggest possible avenues for future research on epitaxially grown light lanthanides.

II. SAMPLE GROWTH AND CHARACTERIZATION

Samples were grown in the University of Illinois EpiCenter using now-standard methods[3] for the growth of rare-earth films and superlattices. Buffer layers of bcc Mo ($\simeq 150$ nm) were first deposited on suitably cleaned epitaxial grade $(11\bar{2}0)$ sapphire substrates at a temperature of 1000 °C and a background pressure of 1×10^{-8} torr. A Y layer, deposited at 700–800 °C with the chamber pressure held at $\simeq 2\times 10^{-10}$ torr, was grown until thick enough to give a clear hexagonal reflection high-energy electron diffraction (RHEED) pattern. Nd and Y were then grown as c-axis superlattices or films, with computer control of the deposition times. A final Y capping layer was added to inhibit oxidation of the highly reactive Nd. Typical growth rates were between 0.03 and 0.1 nm/s.

Because of the small magnetic moment ($\mu_{\rm sat}/\mu_B = 2.6$ as compared with 10.6 for Dy) and multiple domain structure of Nd, samples were grown on 5 cm sapphire wafers in order to obtain a reasonable neutron diffraction signal with an achievable number of bilayers. To improve the homogeneity of the samples, the substrates were rotated at 6 rpm during growth. A total of four thin film samples and eight superlattice specimens were grown. A superlattice not exhibiting a regular bilayer period was annealed at 800 °C for 30 min to form an alloy sample. The true compositions of the superlattice samples were determined from a combination of x-ray and Rutherford backscattering (RBS) data. The superlattice period was determined from the spacing of x-ray superlattice peaks and the atomic fractions from the RBS data. The characteristics of the samples are listed in Table I; in several instances the nominal composition differs substantially from that determined using x rays and RBS. We use the measured compositions in this paper.

The principal goals in the growth of a superlattice structure are regularity of the superlattice period and abruptness at the interfaces. These can be determined by x-ray diffraction studies in the vicinity of Bragg peaks. For a perfect square-wave superlattice with exact matching of the lattice parameters in the direction of growth, each Bragg peak is surrounded by odd-order superlattice harmonics, separated in reciprocal space from that peak by $l \pm 4n/N_\Lambda$, where N_Λ is the total number of atomic planes in a single superlattice bilayer of thickness Λ. The factor 4 arises because we index this and subsequent Bragg peaks relative to a dhcp unit cell

TABLE I. Characteristics of the epitaxial films and superlattices. The notation (b) indicates that the temperature given is that of the bulklike phase. The remaining entries refer to the anomalous, helimagnetic Néel temperature.

Sample	Nominal Nd/Y ratio	Mo buffer (nm)	Y seed (nm)	Y cap (nm)	T_N(K) (SQUID)	T_N(K) (Neutron)
Nd (582 nm)		240	150	12	28±2	< 22 (b)
Nd (156 nm)		165	75	5	25±2	
Nd (11.5 nm)		85	146	8	25±2	
Nd (1.44 nm)		185	70	5		
$[\text{Nd (3.1 nm)}\vert\text{Y (2 nm)}]_{315}$	18/20	100	100	30	32±1	37±2
$[\text{Nd (3.2 nm)}\vert\text{Y (2 nm)}]_{120}$	37/30	100	100	30	32±1	29±2
$[\text{Nd (3.9 nm)}\vert\text{Y (3.9 nm)}]_{120}$	38/38	100	100	30	32±1	28±4
$[\text{Nd (4.2 nm)}\vert\text{Y (1.2 nm)}]_{90}$	35/11	100	100	30	29±2	27±3
$[\text{Nd (4.7 nm)}\vert\text{Y (1.9 nm)}]_{109}$	37/20	100	100	30	30±2	25±2
$[\text{Nd (8.7 nm)}\vert\text{Y (2.4 nm)}]_{80}$	77/21	100	100	30	32±2	27±2
$[\text{Nd (11.5 nm)}\vert\text{Y (2 nm)}]_{80}$	115/20	100	100	30	27±2	22±2 (b)
$Nd_{0.62}Y_{0.38}$ (970 nm)		100	alloyed	alloyed	28±1	30±2

which contains four atomic planes. Differences between the thicknesses of the component layers add even-order superlattice harmonics to the spectrum. Figure 3 shows such an x-ray scan for the $[\text{Nd (8.7 nm)}\vert\text{Y (2.4 nm)}]_{80}$ sample ($N_\Lambda \simeq 40$), in the vicinity of the $(00\cdot 4)$ Bragg peak. The solid line through the data is a fit based on the damped rectangular wave model[10] in which successive Fourier components of the concentration and c-axis lattice parameter are multiplied by attenuation factors. Because the Bragg peak from the Y base layer coincides with the first-order superlattice harmonic near $l=4.1$, the least-squares fit was insensitive to relative Nd and Y layer thicknesses and lattice parameters but was sensitive to the concentration attenuation factor. The fit in Fig. 3 uses the RBS-determined relative thicknesses indicated in the sample designation. The analysis clearly shows that the full width of the interfaces is less than 6 atomic planes.

The $(00\cdot l)$ scan of Fig. 3 cannot differentiate between hcp and dhcp stacking sequences, as the c-axis layer separations are equal for the two structures. The difference is distinguishable, however, in off-axis scans such as $(10\cdot l)$. An hcp crystal, if indexed on the dhcp unit cell, exhibits Bragg peaks only at even-integer values of l, while dhcp stacking results in both even and odd order peaks. Figure 4 is such an x-ray scan on the same sample as in Fig. 3. Arrows indicate those peaks due to dhcp stacking. The width of odd-order peaks corresponds to a coherence length of $\simeq 7$ nm, comparable to the 8.7 nm thickness of each Nd layer, suggesting that they are entirely due to the dhcp Nd layers. The larger atomic number of Nd ($Z=60$) makes these similar in intensity to the even-order peaks to which both Nd and Y ($Z=39$) layers contribute. We conclude, therefore, that the Y layers are hcp and the Nd layers, dhcp as in the bulk materials.

The magnetic properties of each film and superlattice were measured using superconducting quantum interference

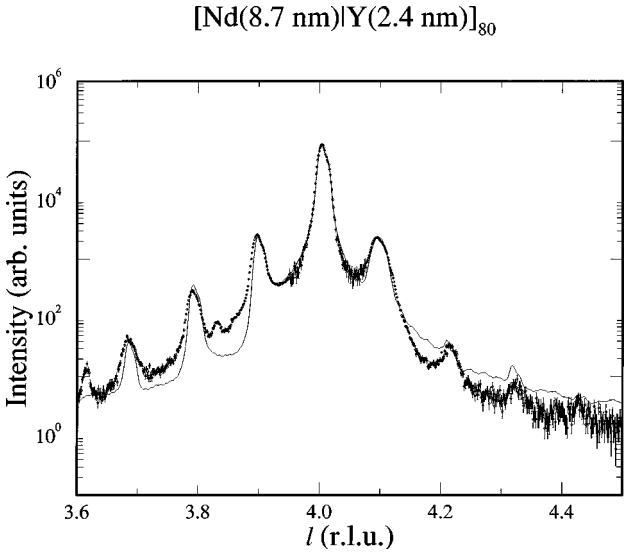

FIG. 3. X-ray scan along **c*** of a $[\text{Nd (8.7 nm)}\vert\text{Y (2.4 nm)}]_{80}$ superlattice. The solid line compares the data to a profile based on the diffusion model.

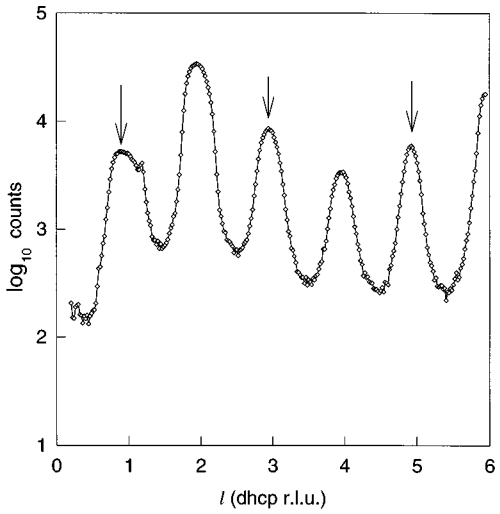

FIG. 4. X-ray diffraction scan along the $(10\cdot l)$ axis of a $[\text{Nd (8.7 nm)}\vert\text{Y (2.4 nm)}]_{80}$ superlattice. The peaks indicated by arrows are due entirely to the Nd interlayers. The breadth of the peaks is consistent with hcp and dhcp structures alternating in the Y and Nd layers, respectively.

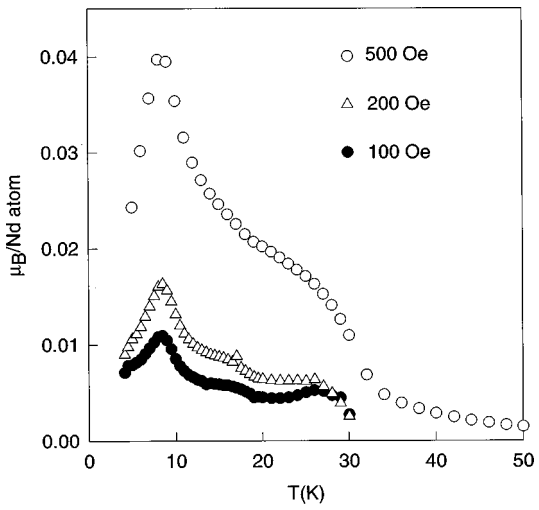

FIG. 5. Zero-field cooled magnetization of the 582 nm Nd film with the field along the (100) easy axis. The anomaly near 27 K is associated with the Néel point, which is significantly higher than in bulk Nd; the peak near 8 K arises from cubic-site ordering.

device (SQUID) magnetometry. Small segments ($\simeq 10$ mm^2) were cut from samples using a diamond wire saw and, to reduce background contributions, were cemented to a long Kapton band with a small amount of wax or epoxy. The principal remaining background contribution arises from the 20 mg sapphire substrate, which has a diamagnetic moment of $\simeq 10^{-5}$ emu in a field of 1 kOe; the signal from 100 nm of Nd is approximately an order of magnitude larger. Figure 5 shows the magnetic moment per Nd atom for the Nd (582 nm) film upon warming in several fields applied along the **b** axis after being cooled to 4.2 K in zero field (ZFC). Well-defined anomalies are observed at 8 K and near 27 K in the lowest field, associated presumably with the ordering of the cubic sites and the Néel temperature T_N, respectively. Comparable data for the superlattice sample $[\text{Nd (3.2 nm)}|\text{Y (2 nm)}]_{120}$ are shown in Fig. 6 along with field-cooled (FC) data obtained upon cooling in the same field. There is no obvious feature associated with cubic-site ordering above 4.2

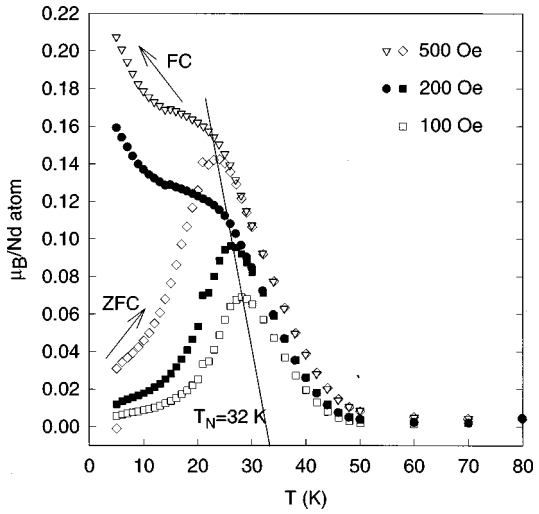

FIG. 6. Field-cooled and zero-field cooled data on a $[\text{Nd (3.2 nm)}|\text{Y (2 nm)}]_{120}$ superlattice. The Néel temperature extrapolates to a zero-field value of 32 K, much above the bulk value of 19.9 K.

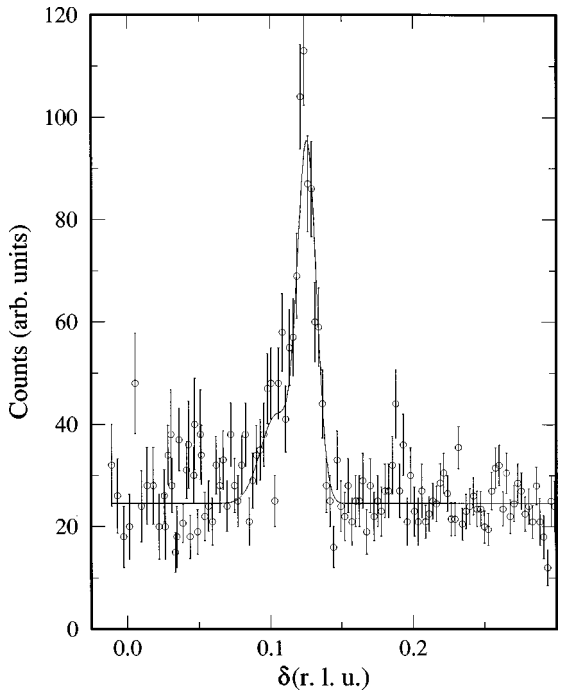

FIG. 7. Neutron diffraction scan along $(\delta 0 \cdot 3)$ at 6 K for the 582 nm film. The peak at $\delta = 0.12$ is close to that associated with hexagonal-site ordering in the bulk. Although evidence of cubic-site order is seen in Fig. 5 for this sample, no peak is evident in the scan.

K in the superlattice. We have extrapolated the peaks in Fig. 6 to zero applied field in order to estimate the true T_N. The Néel points obtained from similar graphs are listed for all of the samples in Table I. Note that T_N in films, and especially in superlattice samples, is significantly higher than that of elemental Nd, a point we return to below.

III. NEUTRON SCATTERING RESULTS

Neutron diffraction data were taken on the BT-9 triple-axis spectrometer at the NIST reactor, and on triple-axis spectrometers TAS-1 and TAS-6 at Risø National Laboratory. All of the superlattice samples and the Nd (582 nm) film were studied at NIST. These were mounted in a cryostat with the **a*** $(h0 \cdot 0)$ and **c*** $(00 \cdot l)$ axes in the scattering plane. A similar configuration was used to examine the $Nd_{0.62}Y_{0.38}$ alloy at Risø. In order to improve the resolution in the **a*** direction, superlattice sample $[\text{Nd (11.5 nm)}|\text{Y (2 nm)}]_{80}$, previously studied at NIST, was mounted with the **a*** and **b*** $(0k \cdot 0)$ axes in the scattering plane at Risø. In this $l = 0$ geometry we cannot detect any component of the ordering wave vector along **c***; furthermore, the ordering of cubic sites is unobservable, as the structure factor is zero for l even.[8]

Figure 7 shows magnetic scattering from the thick Nd (582 nm) film taken at 6 K in the **a***-**c*** geometry. In this $(\delta 0 \cdot 3)$ scan, with δ the scan variable, the peak was observed at the point $\delta = 0.12$ close to $\mathbf{q}_{1,2}$ in Fig. 2(c). The resolution in the **b*** direction is 0.02 nm^{-1} in this geometry, so we cannot resolve any **b*** component of these two wave vectors. If all domains are equally present, the integrated intensity of this peak should represent 1/3 of the total magnetic intensity

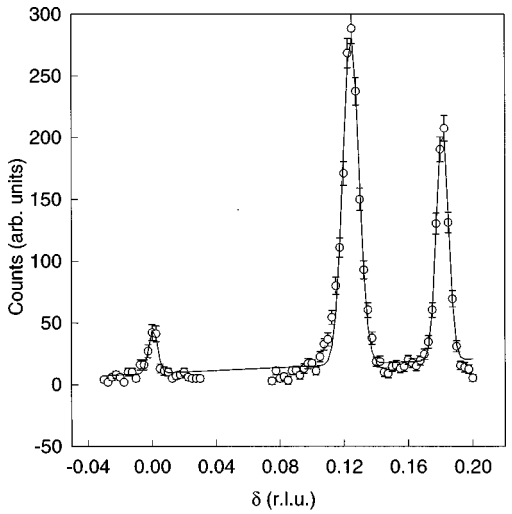

FIG. 8. Neutron diffraction scan along $(\delta 0 \cdot 3)$ at 1.5 K on a [Nd (11.5 nm)|Y (2 nm)]$_{80}$ superlattice. The peaks at $\delta_1 = 0.12$ and $\delta_2 = 0.18$ are consistent with hexagonal- and cubic-site order, respectively. The peak at (003) is not observed in bulk Nd.

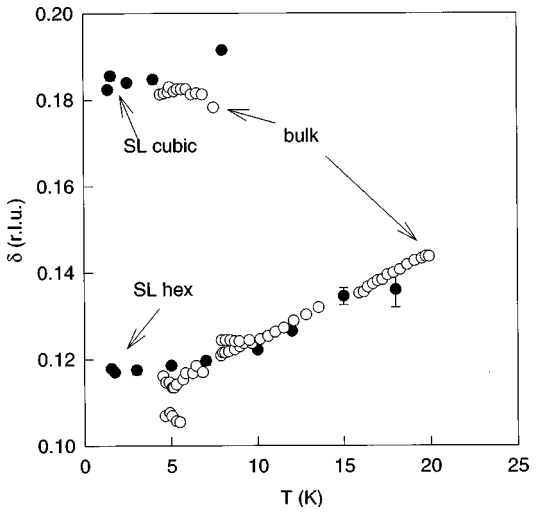

FIG. 9. Positions of the $(\delta_1 03)$ and $(\delta_2 03)$ peaks for the [Nd (8.7 nm)|Y (2.4 nm)]$_{80}$ superlattice (filled circles) along with the hexagonal- and cubic-site peaks of bulk Nd (open circles).

due to hexagonal-site ordering. A comparison of magnetic and structural peaks at 9 K leads to an estimated moment of $2.6 \pm 0.5 \mu_B$ per Nd atom for the film. This is consistent with the high-field saturation moment of $2.2 \mu_B$ per Nd atom[11] and the neutron scattering results[9] but is smaller than the free Nd moment of $3.27 \mu_B$. Though there is a clear anomaly at 8 K in the SQUID data (Fig. 5), the 6 K neutron data show, at most, a weak peak associated with cubic site ordering at $\mathbf{q}_3$. The splitting of $\mathbf{q}_1$ and $\mathbf{q}_2$ [Fig. 2(d)] that occurs at 6.2 K in the bulk, is evident here. The magnetic peak disappears between 15 and 22 K, suggesting that the SQUID anomaly near 27 K is either not associated with magnetic order, or arises from problems in thermometry. We note for later reference that no increase in intensity occurs near $\delta = 0$, and therefore that the thick film orders in a manner similar to bulk Nd.

The situation is quite different for superlattice samples. Figure 8 shows a scan taken at 1.5 K on the superlattice [Nd (11.5 nm) | Y (2 nm)]$_{80}$ with the largest Nd:Y ratio. At this temperature a magnetic peak from the hexagonal sites at $\delta = 0.12$ (but not its splitting) and from the cubic sites at $\delta = 0.18$ are readily observed. An unexpected peak occurs, however, at $\delta = 0$, a feature seen in neither pure Nd nor dhcp Nd/Pr alloys. The bulklike Bragg peaks are sufficiently intense and well resolved that we can compare $\mathbf{q}_1$and $\mathbf{q}_3$ as functions of temperature with values for bulk Nd, as shown in Fig. 9 for [Nd (8.7 nm)|Y (2.4 nm)]$_{80}$. Figure 10 shows the temperature dependence of the magnetic peaks for [Nd (4.2 nm)|Y (1.2 nm)]$_{90}$. As in bulk Nd the $\delta \neq 0$ peaks disappear in the vicinity of 20 K (Refs. 11,12) while the $\delta = 0$ peak persists to higher temperatures. In this sample, both cubic-site ordering, giving rise to the peak at $\delta \simeq 0.18$, and the splitting of the hexagonal-site peak by 0.01 r.l.u. along $\mathbf{a}^*$ [cf. Fig. 2(d)], are apparent in the 5 K data.

While the unbroken scans in Fig. 10 were taken along $(\delta 0 \cdot 3)$, the remaining scans through the anomalous peak were taken at positions $l \neq 3$ that maximized its intensity. A scan along $(00 \cdot l)$ (Fig. 11) on [Nd (4.2 nm)|Y (1.2 nm)]$_{90}$, clearly reveals the c-axis structure to be *incommensurate*; it should be indexed as $(00 \cdot 4 - \tau)$ with τ temperature dependent. The same peak is observed in all superlattice samples. Figure 12 is a plot of the position of the peak as a function of temperature for [Nd (3.2 nm)|Y (2 nm)]$_{120}$ (circles) and [Nd (3.9 nm)|Y (3.9 nm)]$_{120}$ (squares). The c-axis wave vector increases from $\tau \simeq 0.8$ at T_N toward $\tau = 1$ at low temperatures. One interpretation of the data is that a ferromagnetic component of the magnetic moment develops in each Nd plane with successive planes rotated through a turn angle of 72° to form a c-axis helix at T_N. Alternatively, if only the hexagonal sites are involved, the turn angle is twice as large, tending toward antiparallel alignment of successive hexagonal-site planes at lower temperatures. We refer to these incommensurate reflections as helimagnetic peaks in

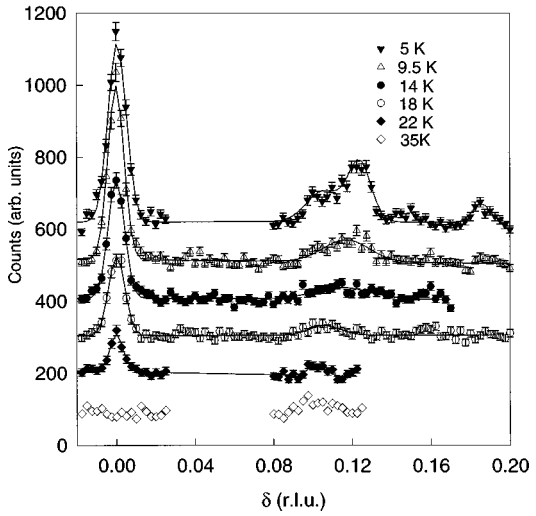

FIG. 10. Successive neutron diffraction $(\delta 03)$ scans (offset vertically) on the [Nd (4.2 nm)|Y (1.2 nm)]$_{90}$ superlattice. The hexagonal-site peak is split at 5 K as in Fig. 2(d). The (003) peak remains observable well above the bulk Néel temperature, consistent with the magnetization data. In these scans, the l index was always set to maximize the intensity of the $\delta \neq 0$ feature. Where there is a gap in the data, the spectrometer was reset to maximize the intensity at $\delta = 0$.

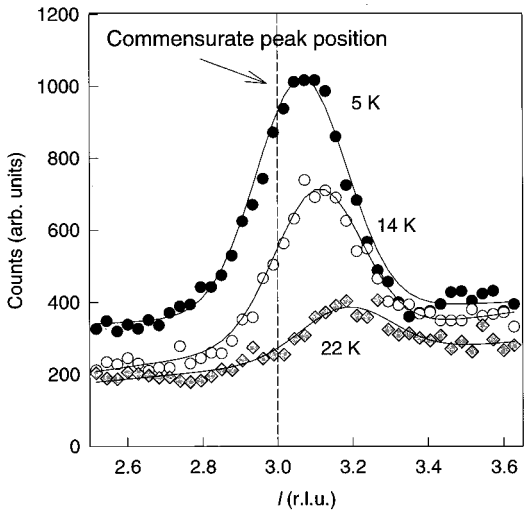

FIG. 11. Scans along $(00l)$ for the [Nd (4.2 nm)|Y (1.2 nm)]$_{90}$ superlattice. The peak is clearly shifted from the commensurate $(00\cdot3)$ position, even at 5 K.

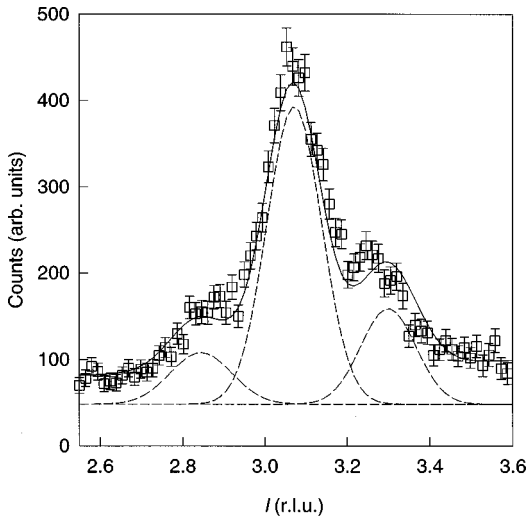

FIG. 13. A $(00l)$ scan, similar to Fig. 10, at 1.6 K for the short-period superlattice [Nd (3.1 nm)|Y (2 nm)]$_{315}$. Magnetic superlattice harmonics are nearly resolved; the widths of the three peaks separated by $2\pi/\Lambda$ give a c-axis magnetic coherence length of 7 nm, approximately two bilayer periods.

analogy to the ordering of heavy lanthanides and their alloys with yttrium.

Comparing the 5 K data in Fig. 10 with those in Fig. 11, we see that the helimagnetic peak is much broader in the **c*** direction than along **a***. One interpretation is that the width measures c-axis magnetic coherence which, after deconvolution of the instrument resolution, is only 4 nm for this sample—essentially limited to a single Nd layer. Indeed, the width in the **c*** direction increases as the Nd-layer thickness is decreased. However, in the sample with the thinnest Nd layer ([Nd (3.1 nm)|Y (2 nm)]$_{315}$), the peak develops well-defined shoulders in the **c*** direction, as the 1.5 K data in Fig. 13 show. The dashed lines show a fit to three Gaussians spaced to agree with the structural superlattice periodicity (0.23 r.l.u.) and a width corresponding to a magnetic correlation length of $\simeq 7$ nm, indicating that helimagnetic order extends over at least two Nd/Y bilayers. No evidence of coupling through the Y spacer layers is seen in the bulklike $\delta \neq 0$ peak, which is found only in samples with larger Nd/Y ratios. A similar sample, [Nd (3.2 nm)|Y (2 nm)]$_{120}$, also has a distinctly non-Gaussian line shape which can be well represented by three superlattice harmonics whose widths correspond to a coherence length of 8 nm and also suggests that the incommensurate magnetic structure couples through at least one Y spacer layer.

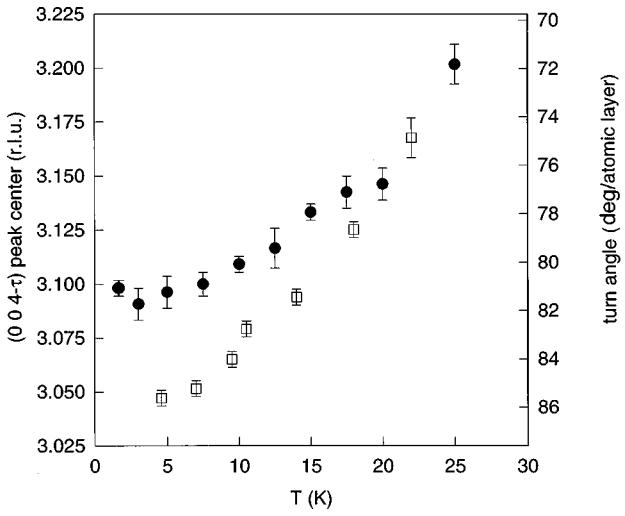

FIG. 12. Position of the helimagnetic peak in [Nd (3.2 nm)|Y (2.0 nm)]$_{120}$ (filled circles) and [Nd (3.9 nm)|Y (3.9 nm)]$_{120}$ (squares) superlattices vs temperature. We index these peaks as $(00\cdot4-\tau)$, with τ both sample and temperature dependent.

The question arises immediately whether the helimagnetic structure is unique to superlattices. To investigate this, we annealed a superlattice sample to form a $Nd_{0.62}Y_{0.38}$ (970 nm) alloy. Neutron scattering studies showed this alloy to have the dhcp structure and to order in the helical phase below 30 K. Helimagnetic peaks were observed at $(00\cdot4\pm\tau)$ and at (00τ), with $\tau = 0.67 \pm 0.03$ throughout the ordered temperature range. Interpreted as a helix, the turn angle is $60\pm1°$ per atomic plane (including cubic sites), in contrast to the 70–90° per plane in the superlattices (Fig. 12). A 60° per plane lock-in state is expected if the moments are aligned parallel to hexagonal crystal axes with no spin slips. We note that this turn angle is relatively close to the 51° per plane usually observed in dilute lanthanide-Y alloy. There is no additional intensity at $(\delta 0\cdot3)$ for $\delta \neq 0$.

We can extract absolute magnetic moments from the data by comparing the integrated intensity of the $(00\cdot4-\tau)$ magnetic peak with the $(00\cdot4)$ Bragg peak. The results are shown in Figs. 14(a) and 14(b) for several superlattices and the alloy sample, assuming here that *all* Nd atoms participate in helimagnetic order. The Néel temperatures estimated from these curves are in reasonable agreement with the zero-field extrapolations from the magnetization data, and are listed in Table I. As the Nd concentration is decreased, the per atom moment associated with helimagnetic order increases while that associated with bulklike ordering of the hexagonal sites decreases. We demonstrate this in Fig. 15, where we have plotted the low-temperature values of the helimagnetic mo-

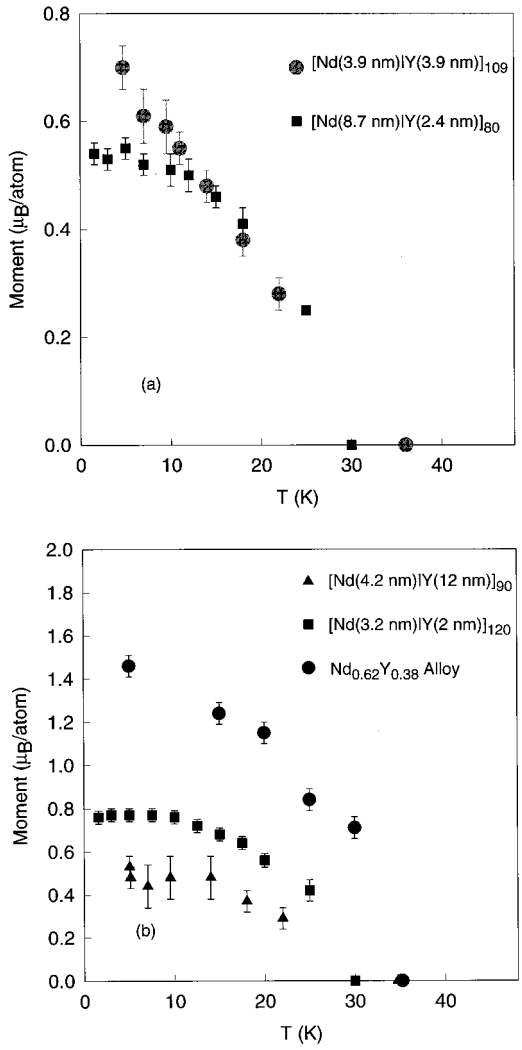

FIG. 14. Temperature dependence of the magnetic moment per Nd atom (hexagonal and cubic sites) that orders in the helimagnetic structure for several superlattices and the alloy sample. The temperatures at which this component vanishes agree semiquantitatively with the Néel temperatures from the magnetization data, as shown in Table I.

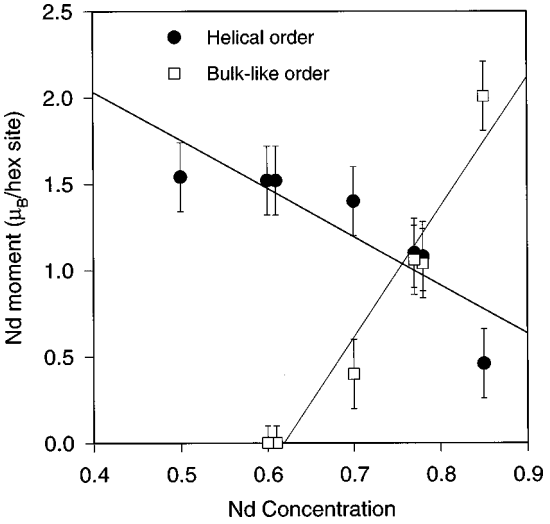

FIG. 15. Magnetic moment per hexagonal site associated with helimagnetic order and the moment per atom associated with bulklike order of hexagonal sites vs the Nd concentration. The Nd atoms are in the dhcp structure in all samples.

ment *per hexagonal site* along with comparable values for the bulklike ordering of hexagonal sites. The sum of the moments is approximately $2.2\mu_B$ where both coexist, reasonably close to fully ordered hexagonal-site moments ($2.6\mu_B$) observed in bulk Nd. In computing the bulklike moment we assumed equal populations of all three possible domains, an assumption we shall see is not necessarily justified. Figures 8 and 10 show that, when the cubic sites order, the intensity is comparable to that of the hexagonal sites, suggesting the coexistence of bulklike and helimagnetic domains and not a more complex magnetic structure exhibiting both types of order. The alloyed sample shows no sign of bulklike order and a significantly larger helimagnetic moment ($2.9\mu_B$ per hexagonal site) than the superlattices, implying some helimagnetic ordering among cubic-site moments.

To explore the multi-**q** structure of superlattices further, sample [Nd (11.5 nm)|Y (2 nm)]$_{80}$ was examined at Risø using a scattering geometry that gives good resolution in both **a*** and **b*** directions. Four of the six magnetic satellites of $(10\cdot 0)$ (cf. Fig. 2) were examined. No evidence of a transverse (**b***) component of the magnetic wave vector such as that in the 4-**q** state of Nd was observed, even at 2.2 K. A puzzling aspect of the data is a marked difference in intensity among symmetrically related peaks. The strongest peak $(1\overline{\delta_1}\cdot 0)$ is roughly a factor 2 more intense than $(1+\delta_1, \overline{\delta_1}\cdot 0)$, which can be attributed to the predominance of one q domain. Indeed, single-**q** structures have recently been detected in magnetic x-ray diffraction from Nd, which measures sample volumes comparable to that of our samples.[13] However, the $(1\delta_1\cdot 0)$ peak, which arises from the same predominant domain, is weaker still. We show this in Fig. 16. Note that bulklike order disappears near 20 K, while helimagnetic order, shown in Fig. 10, persists to 30 K or higher.

IV. DISCUSSION

In early magnetization measurements on the Nd-Y alloy system, Sharif and Coles[5] detected a metastable magnetic phase between 60 and 70 % Nd, in the Sm-like crystal structure regime, with a transition temperature near 32 K that they attributed to a ''residual hcp'' phase. We suggest that our epitaxial alloy in that composition range ($Nd_{0.62}Y_{0.38}$) is in the same residual phase, stabilized here by the constraints imposed by epitaxy. Indeed, the high-temperature phase of Sm is itself dhcp, and the phase boundary moves to lower temperatures under pressure; Coles[14] has argued that a similar situation exists for the Nd-Y alloy system. The epitaxial alloy, grown first as a superlattice and then annealed, has dhcp, rather than the proposed hcp, structure and orders magnetically as an incommensurate c-axis helix. The presence of this phase in the $Nd_{0.62}Y_{0.38}$ alloy suggests that the nesting features which characterize the heavy lanthanides and Y, but are absent in elemental Nd, are restored in the dhcp alloy.

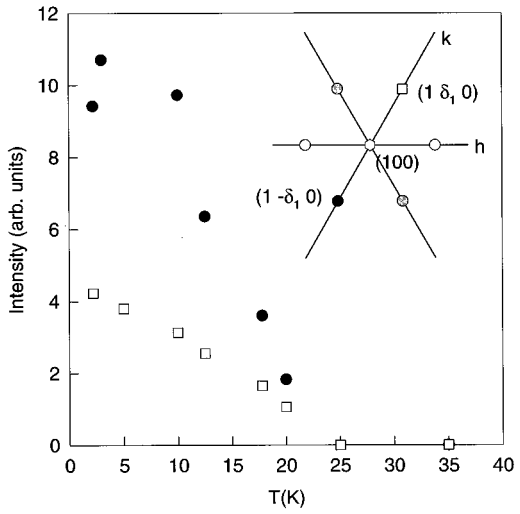

FIG. 16. Integrated intensity of $(1\ \bar{\delta}_1 \cdot 0)$ (circles) and $(1\ \delta_1 \cdot 0)$ (squares) magnetic peaks for $[\mathrm{Nd}\ (115\ \mathrm{nm})|\mathrm{Y}\ (2\ \mathrm{nm})]_{80}$. The large asymmetry suggests that the three possible domains are not equally present. This component of the magnetic order disappears above the bulk T_N but at a temperature at which the helimagnetic component is still present.

Hybridization of the $4f$ levels with the $5d$-$6s$ conduction bands in the lighter rare earths[15] causes the spanning **Q** vector of the nesting regions to increase. As **Q** approaches one-half the distance between the M and L points of the reciprocal lattice, the nesting features can be removed by doubling the unit cell in that direction via dhcp stacking, stabilizing the dhcp structure and suppressing the helical phase.[4] Alloying with Y reduces the f-electron contribution and tends to restore the webbing features. Presumably, this occurs in the concentration range between 30 and 40 at. % Y, and is thought to be responsible for the presence of the intervening Sm crystal structure.[16] However, epitaxial growth of the Nd-Y alloy by annealing an hcp/dhcp superlattice results in a dhcp alloy, which permits us to observe the magnetic order of the dhcp alloy into the Sm-structure region of the phase diagram. The restoration of webbing features increases the conduction electron susceptibility and is also responsible for the increased transition temperatures in the epitaxial alloy and superlattices.

In yttrium-rich superlattices the helimagnetic phase is the predominant magnetic order, with transition temperatures in excess of 30 K. In some samples that exhibit only helimagnetic order, there is evidence for coupling through the Y spacers. Neither helimagnetic nor bulklike order propagates through the spacers when both coexist. The high transition temperature, and the fact that the sum of helimagnetic and bulklike moments is constant within experimental uncertainty, suggests strongly that helimagnetic order arises primarily on the hexagonal-site sublattice, with the moments of successive hexagonal planes tending toward antiferromagnetic alignment at low temperatures. The alloy sample orders similarly, but with a larger moment and a temperature-independent helical pitch. We have suggested, on the basis of the moment and the fact that the turn angle is very close to 60° per atomic plane, that cubic-site moments take part in the helical order of the alloy.

We have considered the possibility that helimagnetic order arises mainly at the interfaces between Nd and Y, and is associated with alloying. However, the two samples having the same helimagnetic moment $(1.1\mu_B)$ and concentration (0.78) in Fig. 15 have quite different Nd-layer thicknesses (4.2 and 8.7 nm). If this were an interface effect, independent of the total Nd-layer thickness, the helimagnetic moment (calculated as the moment per hexagonal site) would be smaller for the sample with the thicker Nd layer, which it is not. Rather, the moment scales with concentration, suggesting that the picture above, in which the two periodicities coexist, is more consistent with the experimental results.

The hexagonal peak at $\delta = 0.12$ is found in the more concentrated superlattices, but neither its splitting nor a Bragg peak associated with cubic-site order are found consistently. One possibility is that existence of the ''archipelago'' Bragg peaks in elemental Nd requires long-range coherence which is limited by the finite regions that exhibit bulklike order. Indeed, even random substitutions of Y at the 6% level suppresses the splitting of the $\delta = 0.12$ peak.[6] We see no regular pattern in the ordering (or lack thereof) of the cubic-site moments and suggest that residual strain, or perhaps c-axis magnetostriction associated with the helical structure, may lower the transition temperature of the cubic sites. These effects are not so profound here as for the heavy rare earths, where magnetoelastic effects play a central role in determining the phase diagram.

Helimagnetic order commonly occurs in dilute alloys of the heavier rare earths with yttrium, and it is therefore not surprising to find it in an Nd-Y alloy that has been stabilized in the dhcp phase. In the case of heavy rare earths layered with nonmagnetic Y or Lu, the local band structure of the magnetic rare earth is approximately preserved, and the observed magnetic structures are closely related to those in the bulk materials. Not so in Nd/Y superlattices, where helimagnetism, absent in bulk Nd, persists over a wide range of Nd- and Y-layer thicknesses, coexisting in some cases with the b-axis spin modulation that is characteristic of the bulk. Despite the fact that the interfaces are abrupt and the stacking alternates between dhcp and hcp, the magnetic structure of the superlattice becomes increasingly that of the alloy as the Y component is increased. Clearly the influence of the nearby Y is paramount and produces a band structure in the Nd similar to that in dhcp Nd-Y alloys. For both the alloy and the superlattices, Fermi-surface nesting is the probable explanation for the observed helical order. Unfortunately, the coherence of the helimagnetic order is limited to a single Nd layer for most of the samples studied. Thus we have no direct measure of the magnetic response of the Y interlayers. As a result, we cannot determine whether this magnetic state indicates bands that belong uniquely to the superlattice or is, alternatively, the result of local perturbations of the bulk Nd band, or even of epitaxial strains. To help clarify these issues, further studies of epitaxially grown Nd/Y alloys are underway.

ACKNOWLEDGMENT

This work was supported in part by the National Science Foundation through Grant No. DMR 94-24339.

[*]Present address: NVE, Inc., Eden Prairie, MN 55344.

[1]W.C. Koehler, in *Magnetic Properties of Rare-earth Metals*, edited by R.J. Elliott (Plenum, London, 1972), p. 117.

[2]J. Jenson and A.R. Mackintosh, *Rare Earth Magnetism* (Clarendon, Oxford, 1991), p. 89.

[3]C.P. Flynn and M.B. Salamon, in *Handbook on the Physics and Chemistry of Rare Earths*, edited by K.A. Gschneidner, Jr. and L. Eyring (Elsevier Science, Amsterdam, 1996), Vol. 22, Chap. 147.

[4]G.S. Fleming, S.H. Liu, and T.L. Loucks, Phys. Rev. Lett. **21**, 1524 (1968).

[5]B. Sharif and B.R. Coles, J. Less-Common Met. **62**, 295 (1978).

[6]S.W. Zochowski, W.G. Marshall, K.A. McEwen, E.M. Forgan, D. Fort, and S. Shaikh, Physica B **180-181**, 26 (1992).

[7]B.A. Everitt, J. A. Borchers, M.B. Salamon, J. J. Rhyne, R. W. Erwin, B.J. Park, and C.P. Flynn, J. Magn. Magn. Mater. **140-144**, 769 (1995); B. A. Everitt, Ph.D. Dissertation, University of Illinois, 1995.

[8]B. Lebech, J. Wolny, and R.M. Moon, J. Phys. Condens. Matter **6**, 5201 (1994).

[9]B. Lebech, K.A. McEwen, and P.A. Lindgård, J. Phys. C **8**, 684 (1975).

[10]R.W. Erwin, J.J. Rhyne, M.B. Salamon, J.A. Borchers, S. Sinha, R-R. Du, J.E. Cunningham, and C.P. Flynn, Phys. Rev. B **35**, 6808 (1987); J.A. Borchers, M.B. Salamon, R.W. Erwin, J.J. Rhyne, R.R. Du, and C.P. Flynn, *ibid.* **43**, 3123 (1991).

[11]K.A. McEwen, G.J. Cock, L.W. Roeland, and A.R. Mackintosh, Phys. Rev. Lett. **30**, 287 (1973).

[12]K.A. McEwen, B. Lebech, and D. Fort, J. Magn. Magn. Mater. **54–57**, 457 (1986).

[13]D. Watson, E.M. Forgan, W.J. Nuttall, W.G. Stirling, and D. Fort, Phys. Rev. B **53**, 726 (1996).

[14]B.R. Coles, J. Less-Common Met. **77**, 153 (1981).

[15]K.A. Gschneidner, Jr., J. Less-Common Met. **25**, 405 (1971).

[16]A. Jayaraman, in *Handbook on the Physics and Chemistry of the Rare Earths*, edited by K.A. Gschneidner, Jr. and L. Eyring (North Holland, Amsterdam, 1978), Vol. 1, p. 707.